

Low Temperature Synthesis of Cu₂O Crystals: Shape Evolution and Growth Mechanism

Yongming Sui,[†] Wuyou Fu,[†] Haibin Yang,^{*,†} Yi Zeng,[‡] Yanyan Zhang,[†] Qiang Zhao,[†] Yangen Li,[†] Xiaoming Zhou,[†] Yan Leng,[†] Minghui Li,[†] and Guangtian Zou[†]

[†]National Laboratory of Superhard Materials, Jilin University, Changchun, 130012, PR China and

[‡]State Key Laboratory on Integrated Optoelectronics, College of Electronic Science and Engineering, Jilin University, Changchun 130012, PR China

Received April 20, 2009; Revised Manuscript Received November 8, 2009

ABSTRACT: An interesting shape evolution of Cu₂O crystals, that is, from cubes, truncated octahedra, octahedra, and finally to nanospheres was first realized in high yield by reducing the copper–citrate complex solution with glucose. X-ray powder diffraction (XRD), field-emission scanning electron microscopy (FESEM), and high-resolution transmission electron microscopy (HRTEM) techniques were employed to characterize the samples. We elucidate the important parameters (including poly(vinyl pyrrolidone) (PVP) concentration, reaction time, and reaction temperature) responsible for the shape-controlled synthesis of Cu₂O crystals. The possible formation mechanism for the products with various architectures is presented, which is mainly based on the variation of the ratio (*R*) of the growth rates along the $\langle 100 \rangle$ and $\langle 111 \rangle$ direction. In addition, the effect of the low supersaturation on the formation of star-shaped samples with six symmetric branches is also taken into account. This polymer-mediated method should be readily extended to the controlled synthesis of other metal oxides and the proposed growth model could also be used to explain and direct the growth of crystals with a cubic structure.

1. Introduction

In recent years, developing ways of tailoring the structure of materials on specific morphologies has been one of the important goals of material scientists. The shape and size of inorganic materials are well-known to have great effects on their widely varied properties.¹ To date, much effort has been devoted to synthesize novel nano- and microstructured materials with various shapes, such as low-dimensional structures (e.g., rods,² wires,³ belts,⁴ tubes,⁵ cubes⁶) and hierarchical structures (e.g., dendrites,⁷ branches,⁸ urchins,⁹ networks¹⁰), for their specific properties and corresponding potential applications. If we could understand the growth mechanism and the shape-guiding process, it could be possible to program the system to yield the final crystals with desired shape and crystallinity.¹¹

Cu₂O is a typical p-type direct band gap semiconductor with a band gap of 2.17 eV and has potential applications in solar energy conversion,¹² electrode materials,¹³ sensors,¹⁴ and catalysts.¹⁵ It has also been found that high-intensity photon-excitation can give rise to the coherent propagation of Cu₂O excitons through Cu₂O solid owing to the large exciton binding energy of 150 meV.¹⁶ Furthermore, its potential application in catalysts was demonstrated by the discovery that Cu₂O could act as a stable photocatalyst for the photochemical decomposition of water into O₂ and H₂ under visible light irradiation.¹⁷ Cu₂O nanocrystals with cubic and octahedral geometries are the most interesting, which is because other more complex particle structures can be derived from these simple structural forms, and their well-defined surfaces provide unique opportunities for the examination of their facet-specific properties.¹⁸ Recently, various methods have been reported for the production of Cu₂O with varied

morphologies: Huang et al. have reported the high yield growth of monodispersed Cu₂O nanocubes with approximate average sizes of 40, 65, 100, 230, and 420 nm using a seed-mediated synthesis approach in aqueous solution.¹⁹ Monodispersed nano- and microcubes were prepared by Murphy et al. from the reduction of Cu(II) salts in the presence of poly(ethylene) glycol (PEG, *M_w* = 600) and cetyltrimethylammonium chloride (CTAB) as protecting agents.²⁰ Octahedral Cu₂O crystals with a tunable edge length were synthesized by reducing copper hydroxide with hydrazine,²¹ while nanooctahedral Cu₂O crystals with controllable sizes of ~100 nm have been prepared via γ irradiation in Triton X-100 microemulsions as well as via slow oxidation of Cu under ambient conditions.²² In addition, electrodeposition methods are commonly used to synthesize Cu₂O crystals with various morphologies. Choi et al. have demonstrated a methodological approach for utilizing the preferential adsorption of surfactant during the electrodeposition process to obtain truncated octahedral Cu₂O crystals.²³ Xu et al. have also reported that truncated octahedral Cu₂O crystals can be obtained by adding a small amount of hydrophilic RTILs in the aqueous deposition solution.²⁴

Herein, we report a facile solution-phase route for the mass synthesis of Cu₂O crystals with different morphologies in the presence of poly(vinyl pyrrolidone) (PVP) at relatively mild temperature of 80 °C. In our system, the morphological evolution from cubes to truncated octahedra, octahedra, and nanospheres has been investigated by using different amounts of PVP, which may be attributed to the selective interaction of PVP with $\{111\}$ facets during the reaction. In addition, the formation of star-shaped Cu₂O with six symmetric branches is closely related to the low supersaturation, and the effect of the reaction temperature on the final morphologies and sizes of Cu₂O crystals is also explored in detail. Finally, optical absorption spectra of these Cu₂O

*Corresponding author: Tel.: +86-431-85168763; fax: +86-431-85168763; e-mail: yanghb@jlu.edu.cn.

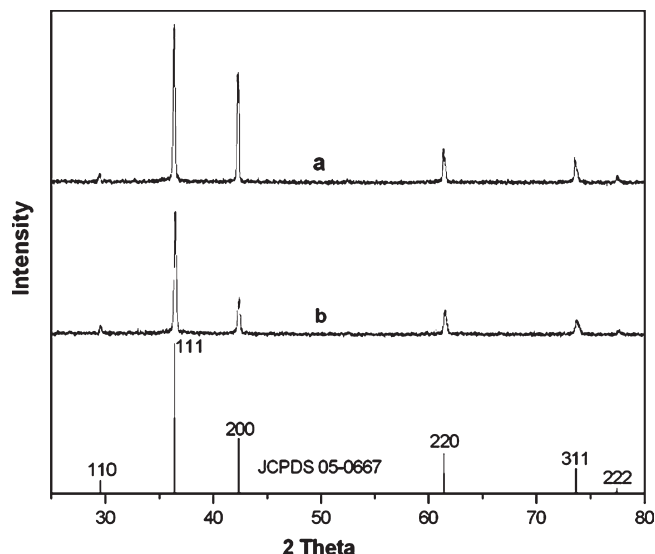


Figure 1. XRD patterns of the Cu_2O cubes (a) and the Cu_2O octahedra (b), as well as the standard data for Cu_2O (JCPDS 05-0667).

crystals are obtained to see how the particle shape affects their absorption characteristics.

2. Experimental Section

Synthesis. All the reagents were purchased from Beijing Chemical Reagent Co. Ltd. and used as received. In a typical procedure, an aqueous solution was first prepared by mixing 17 mL of water, 1 mL of 0.68 M copper sulfate, and PVP (0.3 g; K-30; $M_w = 30\,000$) in a round-bottomed glass flask. The mixture was stirred with a magnetic blender for about 15–20 min, and then 1 mL of 0.74 M sodium citrate and 1.2 M anhydrous sodium carbonate mixture solution was added in a dropwise manner into the above solution. A dark blue solution soon appeared, whereas no precipitate was observed. After about 10 min, 1 mL of 1.4 M glucose solution was slowly dropped into it. The solution was kept in a water bath at a temperature of 80 °C for 2 h, and then cooled to room temperature naturally. The brick red precipitate was filtered off, washed several times with distilled water and absolute alcohol, and finally dried in a vacuum at 60 °C for 8 h. Further experiments were also conducted under different conditions, using procedures similar to those presented above (The detailed experimental conditions are shown in Figure S1, Supporting Information).

Characterization. X-ray powder diffraction (XRD) analysis was conducted on a Rigaku D/max-2500 X-ray diffractometer with $\text{Cu K}\alpha$ radiation ($\lambda = 1.5418 \text{ \AA}$). Field-emission scanning electron microscopic (FESEM) images were performed on a JEOL JEM-6700F microscope operating at 5 kV. Transmission electron microscopic (TEM) images, selected area electron diffraction (SAED) patterns, and high-resolution transmission electron microscopic (HRTEM) images were obtained on a JEOL JEM-2000EX microscope with accelerating voltage of 200 kV and a JEOL JEM-3010 microscopy operated at 200 kV, respectively. UV–vis absorption spectra were recorded using a spectrophotometer (Shimadzu, 3100 UV–vis–NIR).

3. Results and Discussion

3.1. Phase Formation. The composition and phase purity of the products were first examined by XRD, and the results reveal that pure Cu_2O is obtained in all samples. Figure 1 displays the representative XRD patterns of the cubes (Figure 1a) and octahedra (Figure 1b) as well as the standard card (JCPDS No. 05-0667), indicating that all the diffraction peaks are readily indexed to cubic phase Cu_2O (space group: $Pn3m$, $a = 0.4294 \text{ nm}$) with no impurity, such as metallic

copper or cupric oxide. The strong and sharp peaks indicate that the obtained Cu_2O crystals are highly crystalline. Meanwhile, we observe that the intensity ratio between the (111) and (200) diffraction peaks is lower than the ratio of those peaks in the standard powder pattern (1.4 versus 2.7) for cubes, whereas the value (3.05) for octahedra is higher. These results indicate that cubes are abundant in {100} facets, whereas {111} facets should dominate octahedra. It has been known that the facets with a slower growth rate will be exposed more on the crystal surface and consequently exhibit relatively stronger diffraction intensity in the corresponding XRD pattern.²⁵ Therefore, it can be concluded that the relatively slower growth rate for cubes and octahedra of Cu_2O are {100} and {111} facets, respectively. Furthermore, such variations of the intensity ratio suggest anisotropic growth of these planes during the growing processes. These results are further confirmed by the following discussions.

3.2. Morphologies and Growth Mechanism of Cu_2O . Generally, the growth process of crystals is a kinetically and thermodynamically controlled process that can form different shapes with some degree of shape tunability through changes in the reaction parameters.²⁶ In our system, we focus on the effects of PVP concentration, reaction temperature, and reaction time on the final shapes of Cu_2O crystals.

3.2.1. Effects of PVP Concentration. Figure 2 shows both FESEM and TEM images of Cu_2O cubes obtained at 80 °C for 2 h using 0.5 mM PVP. It can be clearly seen that these particles are well-defined cubes with sharp edges and uniform shape. Through the magnified FESEM image of Cu_2O cubes, we can observe that it is mainly composed of six {100} planes and the average edge length is measured to be about 800 nm (Figure 2a). Interestingly, we are able to observe similar-sized cubes with slightly truncated corner. These Cu_2O truncated octahedra can be obtained upon further growth of these cubes (Figure 2b). Further investigation by TEM shows that the cubes form the majority of the products, and a small portion of truncated cubes is also commonly observed in the products (Figure 2c). The fringes in a typical HRTEM image (Figure 1d) are separated by $\sim 0.21 \text{ nm}$, in good agreement with the (100) lattice spacing of Cu_2O . The corresponding FFT pattern (Figure 2d, inset) of a cube exhibits a cubic pattern along the $\langle 100 \rangle$ zone axis.

When the PVP concentration is 1.5 mM and other experimental conditions are kept the same, the morphology of products is recorded by FESEM and TEM with different magnifications as shown in Figure 3. Figure 3a shows a panoramic view of the as-prepared products, from which regular Cu_2O truncated octahedra with narrow size distribution are demonstrated. The mean edge length is measured to be about 300–500 nm. Through the magnified FESEM image of truncated octahedron (Figure 3b), we can observe that it is mainly composed of eight {111} planes and six {100} planes, and the overall structure shares 24 identical edges in a mean way. Furthermore, the products are likely to align along both the $\langle 100 \rangle$ and the $\langle 111 \rangle$ directions normal to the substrate, and a mixture of squares and hexagons appears in the TEM images (Figure 3c,d). The corresponding SAED pattern reveals that they are single-crystal structure (Figure 3d, inset).

Increasing the PVP concentration to 2.5 mM in a separate reaction batch leads to the truncation of the octahedral vertices as seen in Figure 4. In the ideal (truncated) octahedra structure, the surface is covered with both {100} and {111} faces. The (truncated) octahedra are observed with a

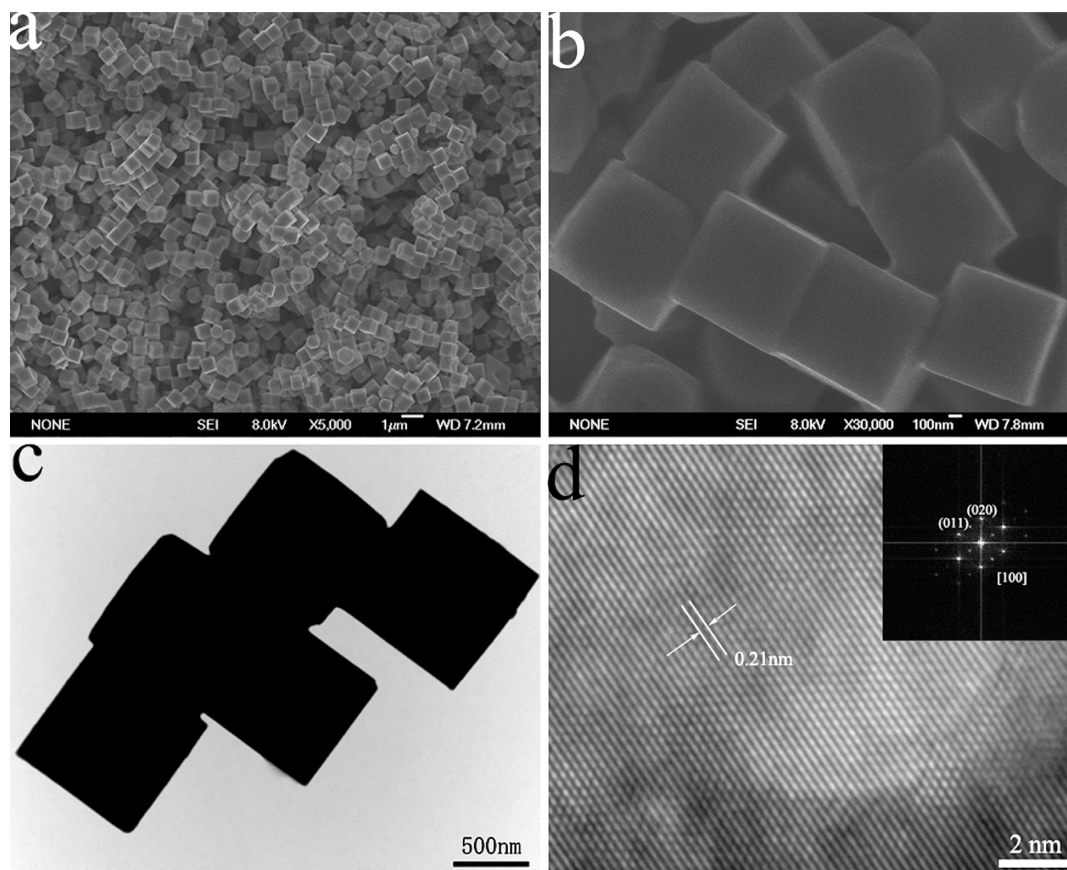


Figure 2. FESEM images (a, b), TEM image (c), HRTEM image and FFT pattern (d) of as-prepared Cu_2O cubes.

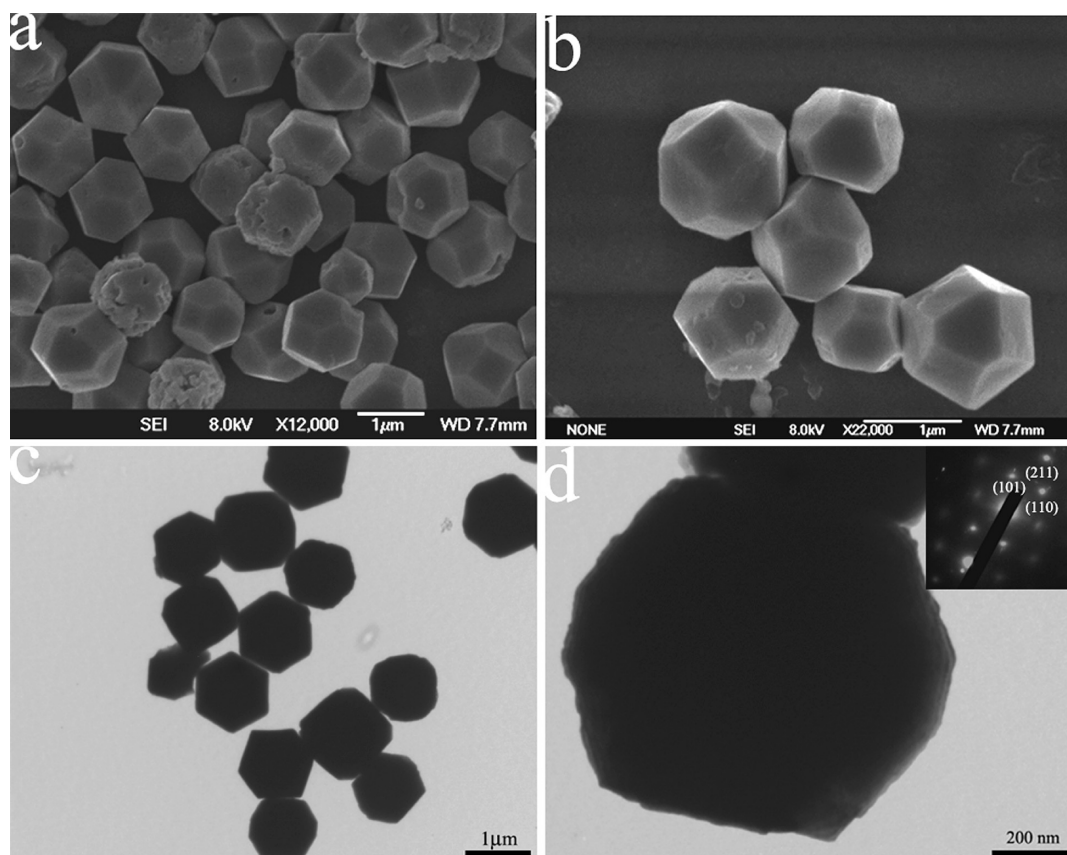


Figure 3. FESEM images (a, b) and TEM image (c, d) of as-prepared Cu_2O truncated octahedra. Inset in (d) is a SAED pattern.

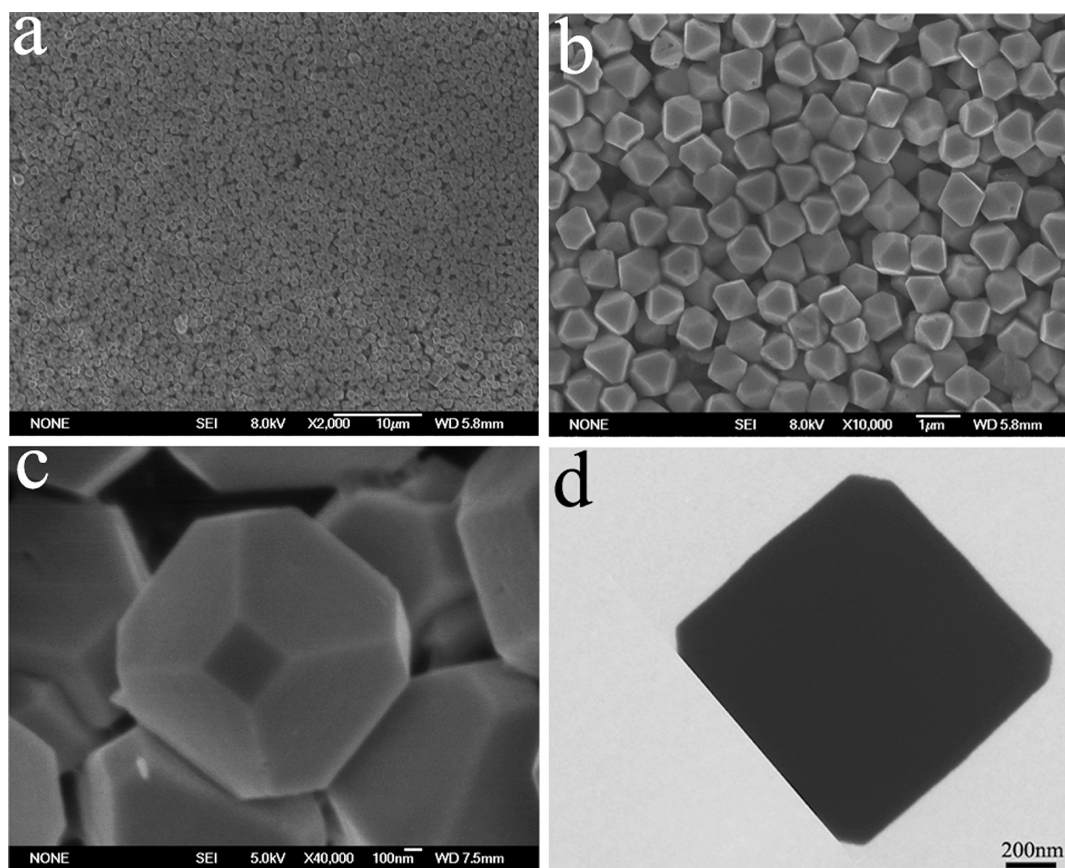


Figure 4. FESEM images (a–c) and TEM image (d) of as-prepared Cu_2O (truncated) octahedra.

side length from 600 to 800 nm and small square facets at the vertices. Obviously, the area ratio of $\{111\}$ and $\{100\}$ faces of the (truncated) octahedra increases because the growth along the (100) plane is quicker than along the (111) plane. Further investigation shows that a cube with truncation appears in the TEM image (Figure 4d).

Fully developed Cu_2O octahedra are observed when the PVP concentration is increased to 4.5 mM. The as-obtained Cu_2O crystals possess perfect octahedral morphology with sharp corners and well-defined edges. The octahedral edge lengths is in the range of 1–1.2 μm , increased from that of the truncated octahedra (Figure 5a,b). Corresponding TEM analysis shows that these octahedral particles project different two-dimensional shapes onto a plane, such as square and rhombus, due to the projection of the octahedra on the TEM grid at a different orientation (Figure 5c,d).²⁷ The SAED pattern indicates that this octahedron is a single crystal of Cu_2O with a $[110]$ -oriented edge lying on the substrate by accident (Figure 5d, inset).

When more PVP (9 mM) was used in the reaction, loose spherical particles with rough surfaces were obtained (Figure 6a,b). The particles are monodispersed with a diameter of 300–400 nm, and the annular SAED pattern indicates that the Cu_2O nanospheres are polycrystalline (Figure 6c,d).

3.2.2. Effects of Reaction Temperature. The influence of reaction temperature on the formation of Cu_2O particles were also investigated, at 70, 90, and 100 $^\circ\text{C}$ for 2 h using 2.5 mM PVP. When the temperature is decreased to 70 $^\circ\text{C}$, the FESEM image (Figure 7a) shows that the Cu_2O truncated octahedra have a similar size distribution to that of the

as-synthesized products at 80 $^\circ\text{C}$ (Figure 5). The difference lies in the fact that nanosized pits are formed on the surfaces and edges. Presumably, the trace oxygen dissolved in solution may gradually oxidize Cu_2O into Cu^{2+} , leading to the formation of pits. A similar phenomenon has also been observed in corrosion-based synthesis of single-crystal Pd nanoboxes.²⁸ When the temperature is increased to 90 $^\circ\text{C}$ (Figure 7b), many ill-defined aggregates are observed in addition to the Cu_2O truncated octahedra due to the high nucleation rate. With a further increase of the reaction temperature to 100 $^\circ\text{C}$, no Cu_2O truncated octahedra are formed; only equiaxial particles with an average size of about 1 μm are formed (Figure 7c). On the basis of our XRD results, a small amount of metallic copper appears, indicating that there is a temperature limit to obtain pure Cu_2O (Figure S2, Supporting Information). The reaction temperature affects not only the reaction but also the nucleation and growth rates of particles.²⁹ So, increasing the reaction temperature enhances the reaction and increases the diffusion rate, or nucleation and growth rates. Hence, ill-defined aggregates and equiaxial particles are more easily formed. These results show that the reaction temperature plays a key role in the formation of Cu_2O crystals.

3.2.3. Effects of Reaction Time. For a complete view of the formation process, we consider the growth process of Cu_2O octahedra when using 4.5 mM PVP at 80 $^\circ\text{C}$. Time-dependent morphology evolution experiments are performed by intercepting intermediate products in different reaction stages of 0.5, 4, 8, 12 h. The Cu_2O crystals including octahedra (Figure 8a,b), star-shaped (Figure 8c,d), and star-shaped with six symmetric branches (Figure 8e,f) are

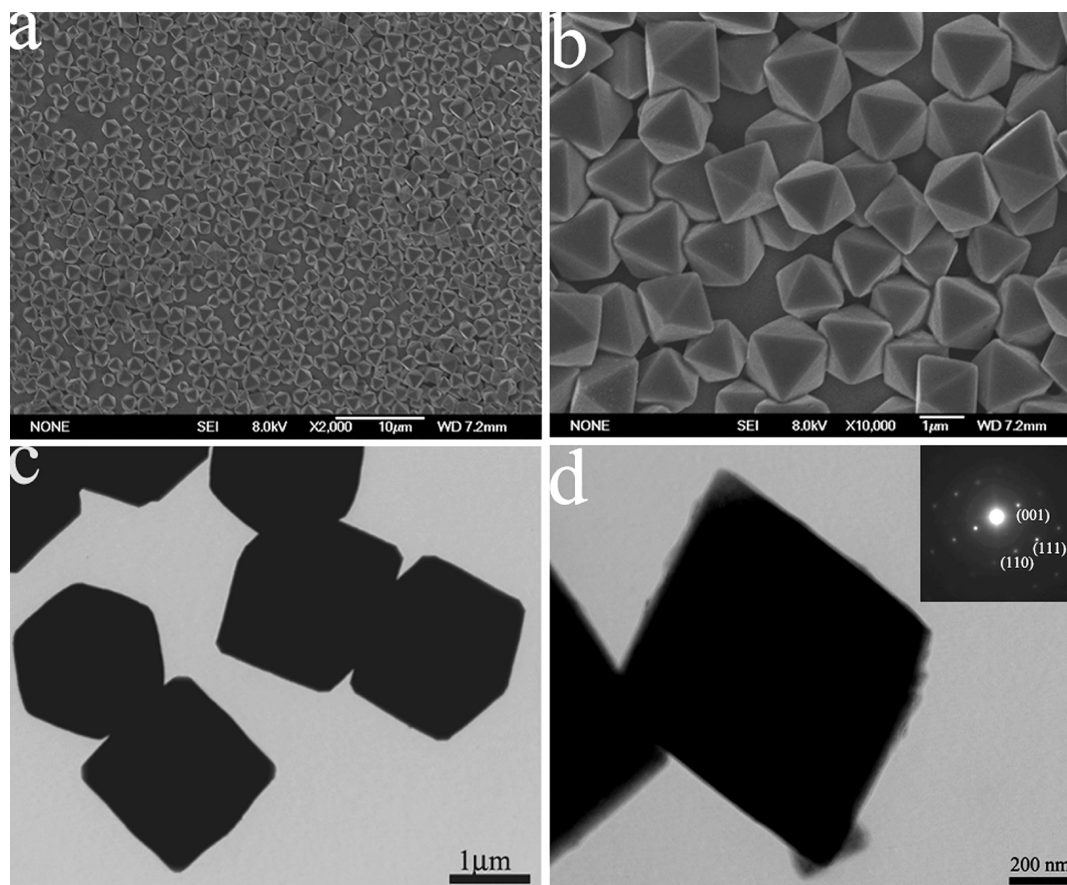


Figure 5. FESEM images (a, b) and TEM images (c, d) of as-prepared Cu_2O octahedra. Inset in (d) is a SAED pattern.

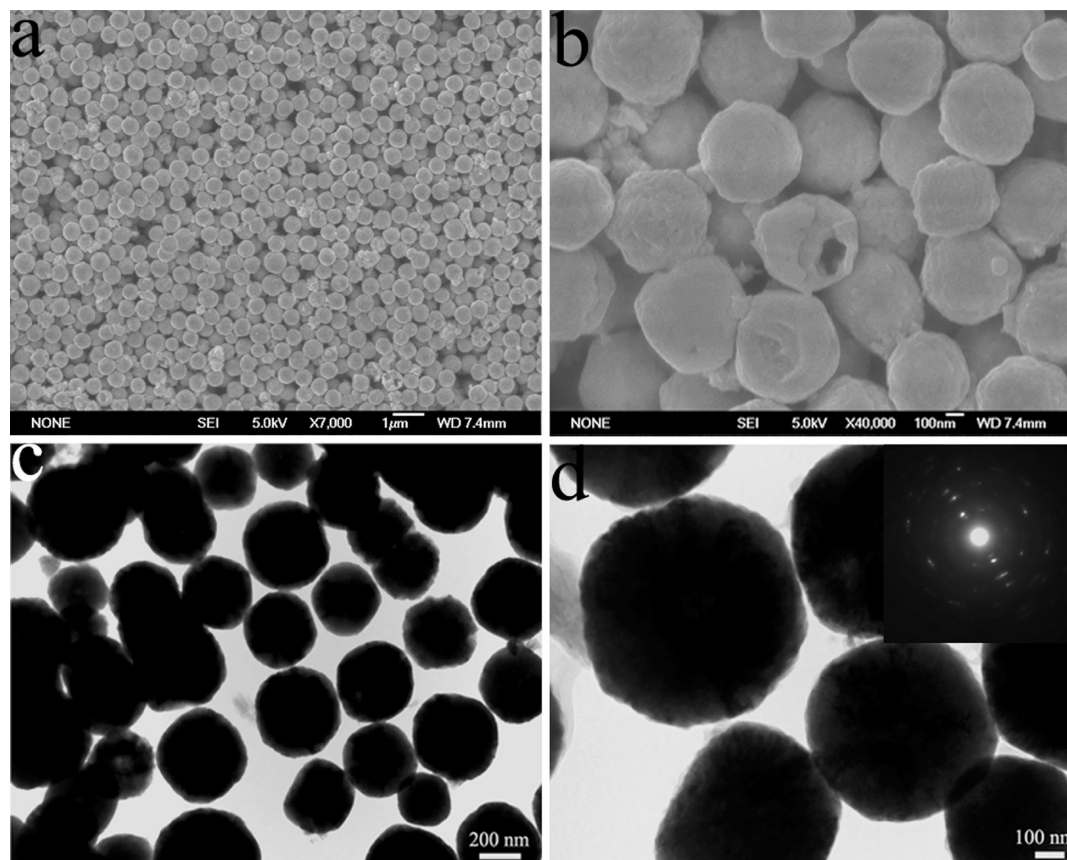


Figure 6. FESEM images (a, b), TEM images (c, d), and corresponding SAED pattern (d, inset) of as-prepared Cu_2O nanospheres.

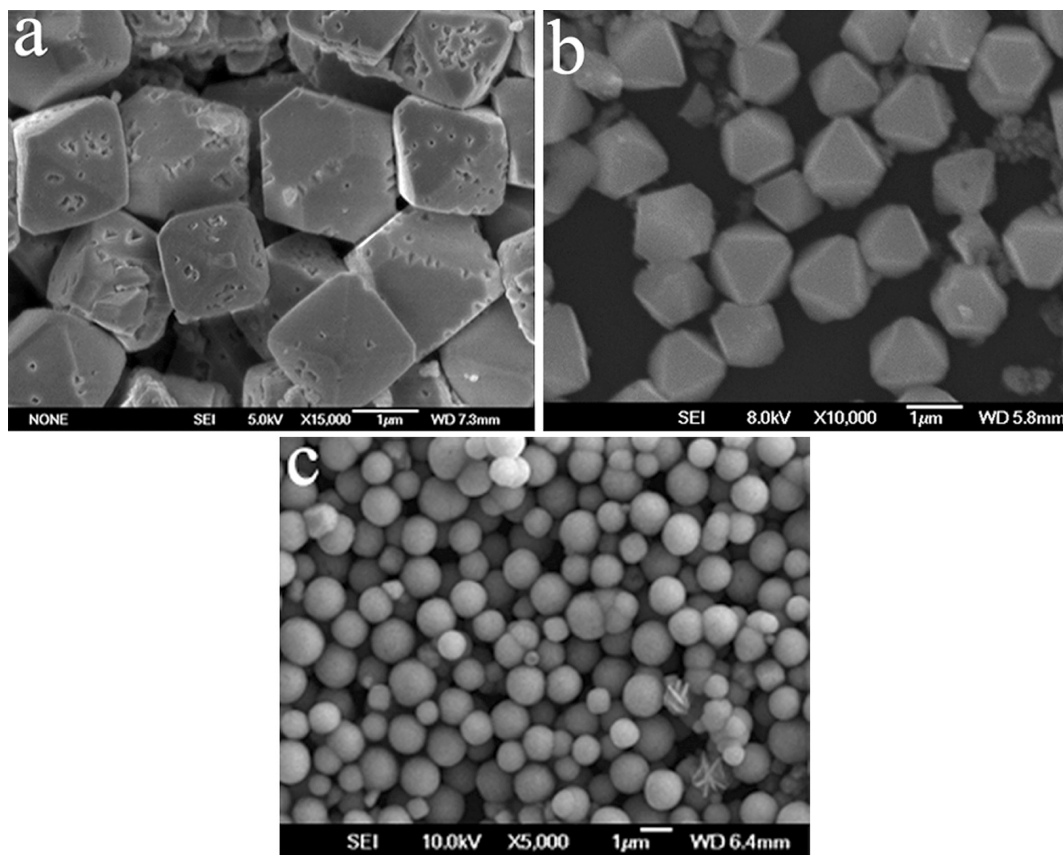
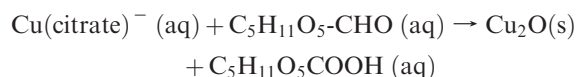


Figure 7. FESEM images of the samples synthesized for 2 h using 2.5 mM PVP at different reaction temperatures: (a) 70; (b) 90; and (c) 100 °C.

obtained. Figure 8 indicates clearly the evolution process of the Cu_2O crystals by varying the reaction time.

When the reaction is carried out for 30 min, it can be seen that all of the obtained particles take on an octahedral-like morphology (Figure 8a,b). Most of the particles are uniform in size with an average edge length of about 500 nm. There are also some small nanooctahedra in the products. When the reaction proceeds for 4 h, certain amounts of well-defined star-shaped geometries with symmetrical horns begin to appear (Figure 8c,d). The particle size determined from the distance between two neighboring vertices is about 2–2.5 μm . However, if the reaction time is further increased to 8 h, the particle size remains unchanged, while the morphology evolves toward star-shaped particles with six symmetric branches (Figure 8e,f). After a reaction time of 12 h, it is clearly found that some star-shaped particles are destroyed, as shown in Figure 8g,h.

3.3. Growth Mechanism. It is well-known that the copper–citrate complex can be reduced by glucose to form Cu_2O precipitates, which are widely used in the analytical determination of saccharides.³⁰ Regular polyhedral Cu_2O particles are synthesized by the solution-phase reaction between the copper–citrate complex and glucose at the appropriate temperature of 80 °C. The chemical reaction is as follows:



At the beginning of the reaction, the spherical Cu_2O particle nucleates. The surface of the Cu_2O particle contains high index crystallography planes, through which the particles connect to each other to decrease the surface energy of

the planes.³¹ As the reaction proceeds, the polyhedral particles grow along the different directions with different growth rates due to their different surface energies.

A baseline for crystal morphology is the equilibrium shape that results from minimizing the anisotropic surface free energy of a crystal under the constraint of constant volume. As is well-known, the equilibrium shape that corresponds to a given γ -plot (γ is the anisotropic interfacial free energy per unit area) is given by the Wulff construction, according to which the shape is an inner convex hull bounded by planes (Wulff planes).³² For the cubic phase, a sequence of $\gamma_{\{111\}} < \gamma_{\{100\}} < \gamma_{\{110\}}$ can be easily deduced from the distances between these three faces and the central Wulff's point.³³ From a crystallographic point of view, Cu_2O is a cuprites structure, and the amount of the Cu^{1+} is twice that of the O^{2-} tetrahedral. The structure can be described as a cubic close packing of copper atoms. The $\{111\}$ and $\{100\}$ surfaces in the Cu_2O crystal lattice are different in the surface atom structures. The $\{111\}$ is a nonpolar surface, while $\{100\}$ is a polar surface.^{34,36} According to Gibbs-Wulff's theorem, both the $\{111\}$ and $\{100\}$ faces can be easily maintained in the final appearance. Generally, growth habits of dipolar Cu_2O crystal are dependent on not only their polar characteristic, but also the supersaturation of the solute. Mcfadyen and Matijevi found that the shape of Cu_2O particle changed from polyhedron to needle when the solute concentrations were rather low.³⁵ Chen et al. also reported that the shape of the Cu_2O particle changed from polyhedron to six-pod-like whisker when the supersaturation of the solution was decreased to a relatively low value.³⁶ These results suggest that crystal growth along the polar directions (the $\langle 001 \rangle$ direction for Cu_2O) is enhanced at relatively lower supersaturation.

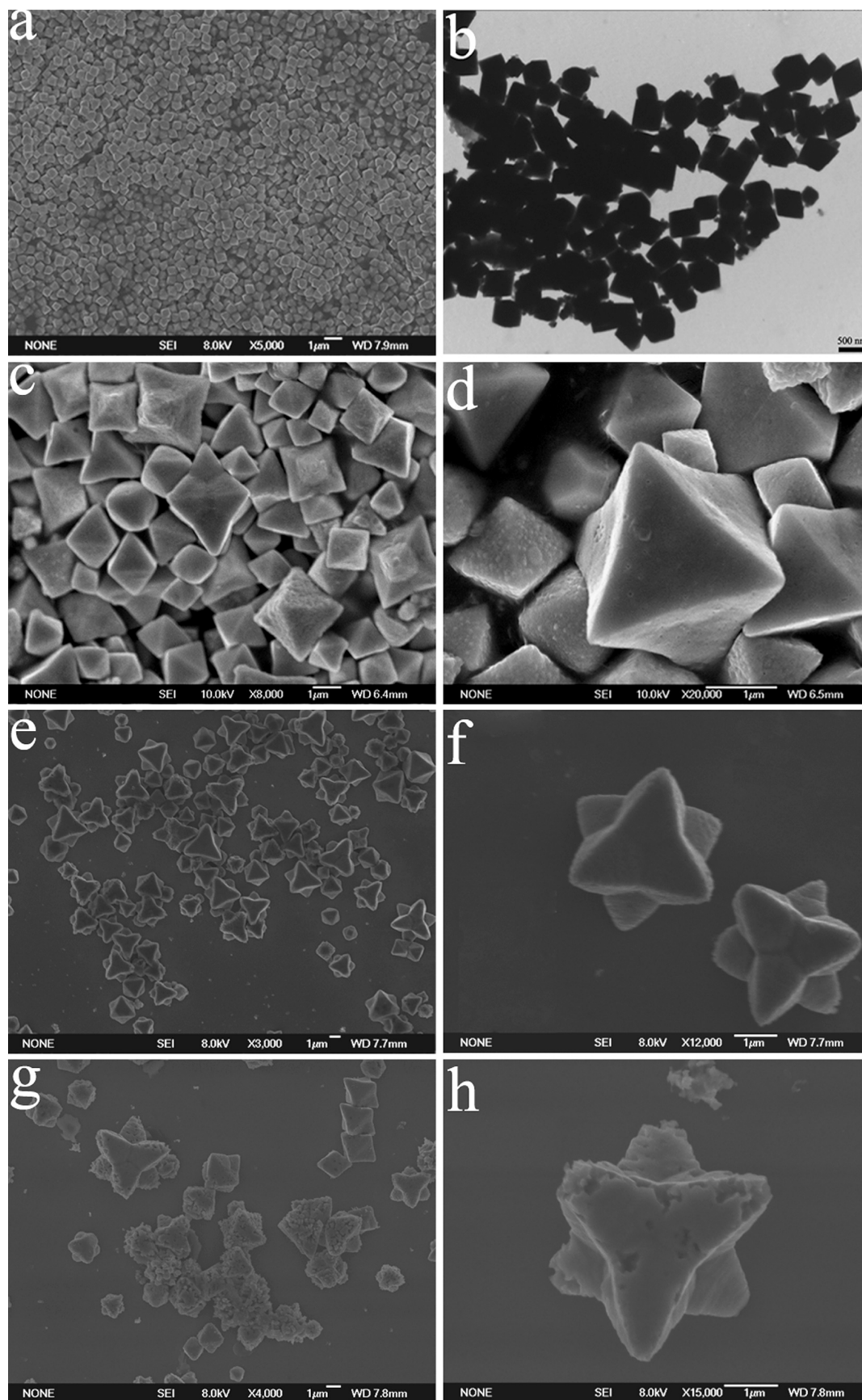
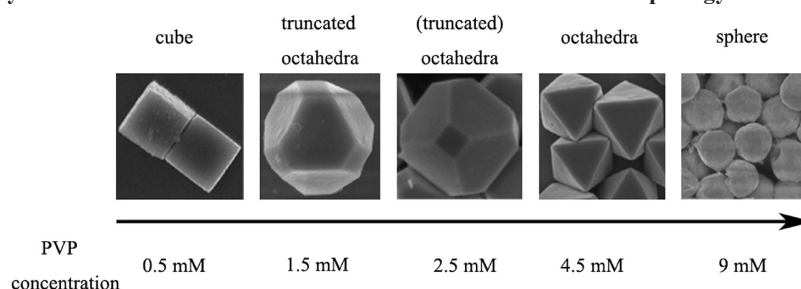
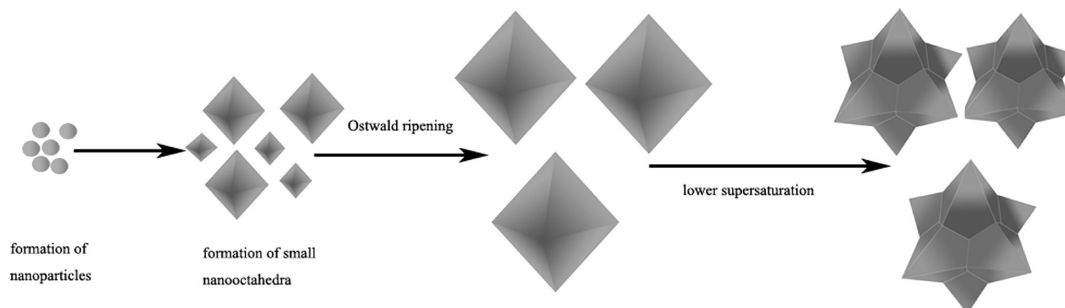


Figure 8. FESEM images of the samples synthesized at 80 °C using 4.5 mM PVP at different reaction times: (a, b) 30 min; (c, d) 4 h; (e, f) 8 h; and (g, h) 12 h.

When inorganic crystals are formed under equilibrium condition, their crystal habit is determined by the relative

order of surface energies.³⁷ The fastest crystal growth will occur in the direction perpendicular to the face with the

Scheme 1. Summary of the Influence of Different Concentration of PVP on the Morphology of the As-Prepared Products**Scheme 2. Schematic Illustration of the Shape Evolution Process of Cu₂O Crystals as a Function of the Reaction Time**

highest surface energy. This results in the elimination of higher-energy surfaces while the lower-energy surfaces increase in area. When organic or inorganic additives are added during the crystal growth process, the relative order of surface energies can be modified.³⁸ Because of anisotropy in adsorption stability, these additives adsorb onto a certain crystallographic plane more strongly than others. This preferential adsorption lowers the surface energy of the bound plane and hinders the crystal growth perpendicular to this plane, resulting in a change in the final morphology. Murphy et al. have reported that the preferential adsorption of molecules and ions in solution to different crystal faces makes the nanoparticles develop into various shapes by controlling the growth rates along different crystal axes.³⁹ A similar phenomenon has been also observed in the shape control of noble metal and other semiconductors with well-defined shapes. For example, as for the synthesis of fcc structured Pd, PVP molecules are adsorbed onto the {100} facets more strongly than onto others, leading to the formation of nanocubes with truncated corners mainly bounded by six {100} facets. Because PVP is a capping polymer, strong interaction exists between the oxygen (and/or nitrogen) atoms of PVP and the {100} facets.⁴⁰ As for the synthesis of cubic structured Cu₂O, it has been demonstrated that the surface energy of the {100} facets of Cu₂O can be selectively lowered relative to that of the {111} facets in the presence of chloride ions, which can stabilize {100} facets and thus induce the formation of single-crystal nanocubes.⁴¹ Moreover, as well demonstrated by Wang,³¹ the ratio (R) of the growth rate along the $\langle 100 \rangle$ to $\langle 111 \rangle$ directions determines the geometrical shape of a crystal. The shape of a cubic nanocrystal will evolve from a perfect cube ($R = 0.58$) to a cuboctahedra ($R = 0.87$), a truncated octahedra ($0.87 < R < 1.73$), and finally to a perfect octahedron ($R = 1.73$) as R increases.

As the reaction proceeds, the polyhedral particles grow along the different directions with different growth rates due to their different surface energies. In the present system,

surfactant PVP could act as not only a stabilizer to prevent the aggregation of the products but also a shape-controller to assist the formation of polyhedral Cu₂O crystals. As a well-known capping or stabilizing agent, PVP molecules with long chains can be adsorbed to the Cu₂O particle surfaces via physical and chemical bonding. When we add PVP into reaction system, it is believed that PVP tends to suppress the growth rate of the {111} planes more than that of the {100} planes, since it interacts more strongly with the {111} facets than with the {100} facets. When a smaller amount of PVP is added to the reaction system, the capping effect of PVP toward Cu₂O particles is weaker or insufficient. Thus, particles with cubic shapes similar to that in the absence of PVP are formed. When the PVP concentration is 1.5 mM, this interaction strength is greatly enhanced, and it could efficiently lower the surface energies of {111} facets. The capping effect of PVP would block the growth on the {111} facets and facilitate the growth on the {100} facets. The obviously different changes of the growth rates on the {100} and {111} facets possibly induce the ratio R to have a value close to 1, leading to the formation of the truncated octahedral Cu₂O crystals. Further increasing the PVP concentration to 4.5 mM, truncated corners ascribed to {100} facets begin to disappear gradually, and even perfect octahedral ($R = 1.73$) are obtained due to the further increase of the growth rate on {100} facets relative to the {111} facets. Finally, spherical particles are generated only when the PVP concentration is 9 mM, owing to the high coverage of PVP on all the planes of Cu₂O nanocrystals. Presumably, the steric effect of PVP against agglomeration and growth is fulfilled and the Cu₂O particles are smaller,⁴² leading to an isotropic growth mode and loose spherical particles. According to this tendency, we can speculate that truncated cubes ($R = 0.7$) and other kinds of cuboctahedra ($R = 0.87$) as intermediate products can be achieved through the regulation of the PVP concentration in the range of 0.5–1.5 mM. This unique role of PVP for the formation of spherical structures evolved from polyhedra is frequently reported in

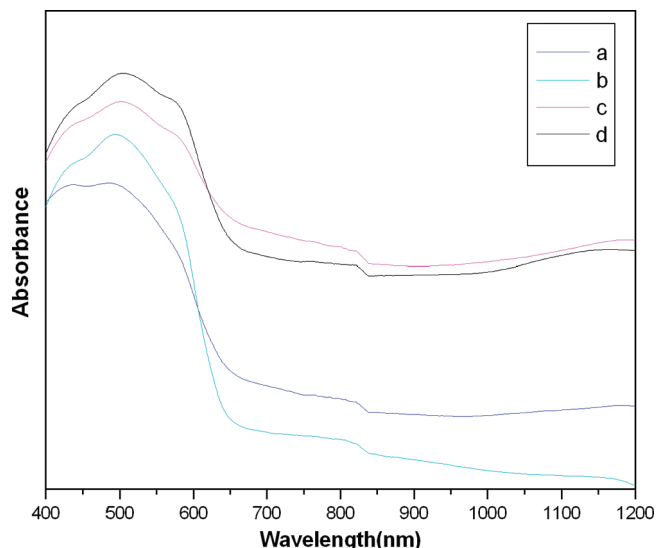


Figure 9. UV-vis absorption spectra of Cu_2O products with different morphologies: (a) cube, (b) truncated octahedra, (c) (truncated) octahedra, (d) octahedra.

previous literature.^{43,29} The whole shape evolution of Cu_2O crystals from cubes to octahedra and finally nanospheres as a function of the PVP concentration is schematically illustrated in Scheme 1.

Generally, the intermediates obtained at different reaction intervals can be used to shed light on the growth mechanism of the crystals. So far, this method is widely used to study the morphological formation of various kinds of crystals under different reaction conditions.⁴⁴ To investigate the formation process of stable Cu_2O octahedral, samples (Figures 5 and 7a,b) at different intervals are prepared with other experimental conditions the same. The octahedral with a diameter of ~ 500 nm and some small nanooctahedra are obtained after a reaction time of 30 min, as shown in Figure 7a,b. This is consistent with the idea that the big octahedra grows from smaller particles. Particle edge sharpening occurs concomitantly with particle growth. With the reaction proceeding to 2 h, the products show uniform octahedra with a narrow size distribution (Figure 5). At this stage, smaller particles are dissolved again and larger particles grow more, which is typical of Ostwald ripening.⁴⁵ Accordingly, the initially formed nanooctahedra can further grow into large ones via Ostwald ripening subsequently. Furthermore, in our system, it is worth noting that when the reaction time is further increased to 8 h, the greatly enhanced growth rate on the $\{100\}$ facets induces the ratio R to have a value of much more than 1.73. Thus, rapid anisotropic growth of the six equivalent $\{100\}$ facets into the six prominent horns results in a six symmetric branches structure. It can be understood based on the following argument: In the nucleus formation stage, nucleation has occurred at relatively high supersaturation, which is favorable for the formation of Cu_2O polyhedra shapes. Thus, the high supersaturation of the solution is decreased to a relatively low value after the solute is consumed for the nucleus formation. As the $\{100\}$ face is dipolar and unstable, apexes growing along the $\langle 100 \rangle$ directions are energetically favorable. To prove this, when the precursor concentration decreased to half, a well-defined star-shaped geometry with symmetrical horns was obtained in the Supporting Information (Figure S3). This preferential growth at six equivalent $\{100\}$ facets eventually leads to the formation

of six symmetric branch structures on the octahedral. The total process is depicted in Scheme 2.

3.4. Optical Properties. Figure 9 shows the UV-vis absorption spectra of Cu_2O products with different morphology including cubes, truncated octahedra, (truncated) octahedra, octahedra. A photograph of cuvettes containing the four Cu_2O solutions is provided in the Supporting Information (Figure S4). The absorption spectra for all the sample are dominated by strong light scattering bands resulting from the relatively large sizes of these crystals.¹⁹ The light absorption band of these Cu_2O crystals at 493 nm for samples cubes, truncated octahedra and at 503 nm for samples (truncated) octahedra, octahedra can be clearly distinguished from the light scattering bands, and the calculated band gap energy of these samples are in the range of 2.46–2.51 eV. This greater band gap value, as compared to that of bulk Cu_2O at 2.17 eV, is attributed to quantum confinement effects.¹⁸

4. Conclusion

In this paper, we present a facile and effective route for the shape-controlled synthesis of Cu_2O crystals via reducing the copper-citrate complex solution with glucose and selective interaction abilities of PVP. A series of morphologies, such as cubes, truncated octahedra, octahedral, and star-shaped particles with six symmetric branches, are easily obtained through the delicate manipulation of the PVP concentration and the reaction time. On the basis of a relatively clear understanding of shape evolution and corresponding growth mechanism, we believe that this polymer-mediated approach can be applied to other shapes and compositions of cubic structure materials.

Acknowledgment. This work was supported by the Natural Science Foundation of China (Grant Nos. 10874053, 50532020) and the National Basic Research Program of China (Grant No. 2005CB724404).

Supporting Information Available: Table 1. Different Synthesis Conditions of Cu_2O Particles. Figure S2. XRD patterns of the Cu_2O synthesized at 100 °C. Figure S3. FESEM images of the samples synthesized for 2 h using 2.25 mM PVP at 80 °C. Figure S4. A photograph of the four solutions showing slight color variation. This information is available free of charge via the Internet at <http://pubs.acs.org/>.

References

- (1) (a) Peng, X.; Manna, L.; Yang, W.; Wickham, J.; Scher, E.; Kadavanich, A.; Alivisatos, A. P. *Nature* **2004**, *404*, 59. (b) Jin, R.; Cao, Y.; Mirkin, C. A.; Kelly, K. L.; Schatz, G. C.; Zheng, J. G. *Science* **2001**, *294*, 1901. (c) Cölfen, H.; Mann, S. *Angew. Chem., Int. Ed.* **2003**, *42*, 2350. (d) Shi, H.; Qi, L.; Ma, J.; Cheng, H. *J. Am. Chem. Soc.* **2003**, *125*, 3450. (e) Lao, J. Y.; Wen, J. G.; Ren, Z. F. *Nano Lett.* **2002**, *2*, 1287. (f) Huang, J. X.; Xie, Y.; Li, B.; Liu, Y.; Qian, Y. T.; Zhang, S. Y. *Adv. Mater.* **2000**, *12*, 808. (g) Xie, Y.; Huang, J. X.; Li, B.; Liu, Y.; Qian, Y. T. *Adv. Mater.* **2000**, *12*, 1523.
- (2) (a) Manna, L.; Scher, E.; Kadavanich, A.; Alivisatos, A. P. *J. Am. Chem. Soc.* **2000**, *122*, 12700. (b) Mayers, B.; Gates, B.; Yin, Y.; Xia, Y. *Adv. Mater.* **2001**, *13*, 1380.
- (3) (a) Zach, M. P.; Ng, K. H.; Penner, R. M. *Science* **2000**, *290*, 2120. (b) Xiong, Y.; Xie, Y.; Li, Z.; Li, X.; Gao, S. *Chem.—Eur. J.* **2004**, *10*, 654. (c) Lu, Q.; Gao, F.; Zhao, D. *Nano Lett.* **2002**, *2*, 725. (d) Greene, L. E.; Yuhas, B. D.; Law, M.; Zitoun, D.; Yang, P. D. *Inorg. Chem.* **2006**, *45*, 7535.
- (4) (a) Dai, Z. R.; Pan, Z. W.; Wang, Z. L. *J. Phys. Chem. B* **2002**, *106*, 902. (b) Liu, Z.; Liang, J.; Li, S.; Peng, S.; Qian, Y. T. *Chem.—Eur. J.* **2004**, *10*, 634.
- (5) (a) Iijima, S. *Nature* **1991**, *354*, 56. (b) Ebbsen, T. W.; Ajayan, P. M. *Nature* **1992**, *358*, 220. (c) Liang, L. F.; Xu, H. F.; Su, Q.; Konishi, H.;

- Jiang, Y. B.; Wu, M. M.; Wang, Y. F.; Xia, D. Y. *Inorg. Chem.* **2004**, *43*, 1594.
- (6) (a) Sun, Y.; Xia, Y. *Science* **2002**, *298*, 2176. (b) Feng, J.; Zeng, H. C. *Chem. Mater.* **2003**, *15*, 2829.
- (7) (a) Chow, A.; Toomre, D.; Garrett, W.; Mellman, I. *Nature* **2002**, *418*, 988. (b) Xiao, J.; Xie, Y.; Tang, R.; Chen, M.; Tian, X. *Adv. Mater.* **2001**, *13*, 1887.
- (8) Roy, V. A. L.; Djuricic, A. B.; Chan, W. K.; Gao, J.; Lui, H. F.; Surya, C. *Appl. Phys. Lett.* **2003**, *83*, 141.
- (9) (a) Shen, G.; Bando, Y.; Lee, C. J. *J. Phys. Chem. B* **2005**, *109*, 10578. (b) Li, B. X.; Rong, G. X.; Xie, Y.; Huang, L. F.; Feng, C. Q. *Inorg. Chem.* **2006**, *45*, 6404.
- (10) Xu, C. X.; Sun, X. W.; Chen, B. J.; Dong, Z. L.; Yu, M. B.; Zhang, X. H.; Chua, S. J. *Nanotechnology* **2005**, *16*, 70.
- (11) (a) Zhou, G. J.; Lü, M. K.; Xiu, Z. L.; Wang, S. F.; Zhang, H. P.; Zhou, Y. J.; Wang, S. M. *J. Phys. Chem. B* **2006**, *110*, 6543. (b) Yang, J.; Lin, C. K.; Wang, Z. L.; Lin, J. *Inorg. Chem.* **2006**, *45*, 8973. (c) Quan, Z. W.; Wang, Z. L.; Yang, P. P.; Lin, J.; Fang, J. Y. *Inorg. Chem.* **2007**, *46*, 1354. (d) Li, C. X.; Quan, Z. W.; Yang, J.; Yang, P. P.; Lin, J. *Inorg. Chem.* **2007**, *46*, 6239.
- (12) Musa, A. O.; Akomolafe, T.; Carter, M. J. *Sol. Energy Mater. Sol. Cell* **1998**, *51*, 305.
- (13) Poizot, P.; Laruelle, S.; Grugeon, S.; Dupont, L.; Taramon, J. M. *Nature (London)* **2000**, *407*, 496.
- (14) Zhang, J.; Liu, J.; Peng, Q.; Wang, X.; Li, Y. *Chem. Mater.* **2006**, *18*, 867.
- (15) (a) Zhang, H.; Ren, X.; Cui, Z. L. *J. Cryst. Growth* **2007**, *304*, 206. (b) White, B.; Yin, M.; Hall, A.; Le, D.; Stolbov, S.; Rahman, T.; Turro, N.; O'Brien, S. *Nano Lett.* **2006**, *6*, 2095.
- (16) Snoke, D. *Science* **1996**, *273*, 1351.
- (17) (a) Hara, M.; Kondo, T.; Komoda, M.; Ikeda, S.; Shinohara, K.; Tanaka, A.; Kondo, J.; Domen, K. *Chem. Commun.* **1998**, 357. (b) de Jongh, P. E.; Vanmaelkelbergh, D.; Kelly, J. J. *Chem. Commun.* **1999**, 1069.
- (18) Kuo, C. H.; Huang, M. H. *J. Phys. Chem. C* **2008**, *12*, 18355.
- (19) Kuo, C. H.; Chen, C. H.; Huang, M. H. *Adv. Funct. Mater.* **2007**, *17*, 3773.
- (20) (a) Gou, L.; Murphy, C. J. *J. Mater. Chem.* **2004**, *14*, 735. (b) Gou, L.; Murphy, C. J. *Nano Lett.* **2003**, *3*, 231.
- (21) Xu, H. L.; Wang, W. Z.; Zhu, W. J. *J. Phys. Chem. B* **2006**, *110*, 13829.
- (22) He, P.; Shen, X.; Gao, H. *J. Colloid Interface Sci.* **2005**, *284*, 510.
- (23) Siegfried, M. J.; Choi, K. S. *Adv. Mater.* **2004**, *16*, 1743.
- (24) Li, H.; Liu, R.; Zhao, R. X.; Zhang, Y. F.; Chen, W. X.; Xu, Z. *Cryst. Growth Des.* **2006**, *6*, 2795.
- (25) Xiong, Y.; Xia, Y. *Adv. Mater.* **2003**, *19*, 3385.
- (26) Quan, Z. W.; Li, C. X.; Zhang, X. M.; Yang, J.; Yang, P. P.; Zhang, C. M.; Lin, J. *Cryst. Growth Des.* **2008**, *8*, 2384.
- (27) Zhang, X. T.; Rao, Y. Y.; Liang, Y.; Deng, R.; Liu, Z.; Hark, S. K.; Yuen, Y. K.; Wong, S. P. *J. Phys. D: Appl. Phys.* **2008**, *41*, 095104.
- (28) Xiong, Y. J.; Wiley, B. J.; Chen, J. Y.; Li, Z. Y.; Yin, Y. D.; Xia, Y. N. *Angew. Chem., Int. Ed.* **2005**, *44*, 7913.
- (29) Li, C. C.; Cai, W. P.; Cao, B. Q.; Sun, F. Q.; Li, Y.; Kan, C. X.; Zhang, L. D. *Adv. Funct. Mater.* **2006**, *16*, 83.
- (30) Petrucci, R. H. *General Chemistry*, 4th ed.; Macmillan Publishing Company: New York, 1985; p 848.
- (31) Wang, Z. L. *J. Phys. Chem. B* **2000**, *104*, 1153.
- (32) (a) Sekerka, R. F. *Cryst. Res. Technol.* **2005**, *40*, 291. (b) Wulff, G. Z. *Krystallogr.* **1901**, *34*, 449. (c) Xu, D.; Xue, D.; Ratajczak, H. J. *Mol. Struct.* **2005**, *740*, 37. (d) Xu, D.; Xue, D. *Physica B* **2005**, *370*, 84. (e) Xu, D.; Xue, D. *J. Cryst. Growth* **2006**, *286*, 108.
- (33) Xu, J. S.; Xue, D. *Acta Mater.* **2007**, *55*, 2397.
- (34) (a) Zhao, H. Y.; Wang, Y. F.; Zeng, J. H. *Cryst. Growth Des.* **2008**, *8*, 3731. (b) Zhao, X. J.; Bao, Z. Y.; Sun, C. T.; Xue, D. F. *J. Cryst. Growth* **2009**, *311*, 711. (c) Islam, M. M.; Diawaro, B.; Maurice, V.; Marcus, P. *Surf. Sci.* **2009**, *603*, 2087. (d) Le, D.; Stolbov, S.; Rahman, T. S. *Surf. Sci.* **2009**, *603*, 1637. (e) Schulz, K. H.; Cox, D. F. *Phys. Rev. B* **1991**, *43*, 1610. (f) Schulz, K. H.; Cox, D. F. *Surf. Sci.* **1991**, *256*, 67.
- (35) Mcfadyen, P.; Matijevic, E. *J. Colloid Interface Sci.* **1973**, *44*, 95.
- (36) Chen, Z. Z.; Shi, E. W.; Zheng, Y. Q.; Li, W. J.; Xiao, B.; Zhuang, J. Y. *J. Cryst. Growth* **2003**, *249*, 294.
- (37) Mullin, J. W. *Crystallization*; Butterworths: London 1971.
- (38) Buckley, H. E. *Crystal Growth*; Wiley: New York 1951.
- (39) (a) Jana, N. R.; Gearheart, L. A.; Murphy, C. J. *Chem. Commun.* **2001**, 617. (b) Jana, N. R.; Gearheart, L. A.; Murphy, C. J. *J. Phys. Chem. B* **2001**, *105*, 4065. (c) Jana, N. R.; Gearheart, L. A.; Murphy, C. J. *Adv. Mater.* **2001**, *13*, 1389.
- (40) Nanda, K. K.; Dahu, S. N. *Adv. Mater.* **2003**, *13*, 280.
- (41) Kim, M. H.; Lim, B. K.; Lee, E. P.; Xia, Y. N. *J. Mater. Chem.* **2008**, *18*, 4069.
- (42) (a) Zhu, H. T.; Wang, T. X.; Xu, G. Y. *Cryst. Growth Des.* **2009**, *9*, 633. (b) Zhu, H. T.; Zhang, C. Y.; Yin, Y. J. *J. Cryst. Growth* **2004**, *270*, 722.
- (43) (a) Gao, J. N.; Li, Q. S.; Zhao, H. B.; Li, L. S.; Liu, C. L.; Gong, Q. H.; Qi, L. M. *Chem. Mater.* **2008**, *20*, 6263. (b) Li, X.; Li, J.; Li, G.; Liu, D.; Chen, J. *Chem.—Eur. J.* **2007**, *13*, 8754.
- (44) (a) Liu, B.; Yu, S. H.; Li, L. J.; Zhang, Q.; Zhang, F.; Jiang, K. *Angew. Chem., Int. Ed.* **2004**, *43*, 4745. (b) Wang, G. Z.; Sæterli, R.; Rervik, P. M.; van Helvoort, A. T. J.; Holmestad, R.; Grande, T.; Rinarsrud, M. A. *Chem. Mater.* **2007**, *19*, 2213. (c) Yu, S. Y.; Wang, C.; Yu, J. B.; Shi, W. D.; Deng, R. P.; Zhang, H. J. *Nanotechnology* **2006**, *17*, 3607.
- (45) (a) Ostwald, W. Z. *Phys. Chem.* **1897**, *22*, 289. (b) Ostwald, W. Z. *Phys. Chem.* **1900**, *34*, 495.